



## Structure and magnetic properties of the $\text{Al}_{1-x}\text{Ga}_x\text{FeO}_3$ family of oxides: A combined experimental and theoretical study

Rana Saha<sup>a</sup>, Ajmala Shireen<sup>a</sup>, A.K. Bera<sup>b</sup>, Sharmila N. Shirodkar<sup>a</sup>, Y. Sundarayya<sup>a</sup>, Nandakumar Kalarikkal<sup>a</sup>, S.M. Yusuf<sup>b</sup>, Umesh V. Waghmare<sup>a</sup>, A. Sundaresan<sup>a,\*</sup>, C.N.R Rao<sup>a,\*</sup>

<sup>a</sup> Chemistry and Physics of Materials Unit, New Chemistry Unit, Theoretical Science Unit and International Centre for Materials Science, Jawaharlal Nehru Centre for Advanced Scientific Research, Bangalore 560 064, India

<sup>b</sup> Bhabha Atomic Research Centre, Trombay, Mumbai 400 085, India

### ARTICLE INFO

#### Article history:

Received 6 December 2010

Accepted 30 December 2010

Available online 5 January 2011

#### Keywords:

$\text{AlFeO}_3$

$\text{GaFeO}_3$

Ferrimagnetism

Cation disorder

Neutron diffraction

Metal oxide

Mössbauer spectroscopy

### ABSTRACT

Magnetic properties of the  $\text{Al}_{1-x}\text{Ga}_x\text{FeO}_3$  family of oxides crystallizing in a non-centrosymmetric space group have been investigated in detail along with structural aspects by employing X-ray and neutron diffraction, Mössbauer spectroscopy and other techniques. The study has revealed the occurrence of several interesting features related to unit cell parameters, site disorder and ionic size. Using first-principles density functional theory based calculations, we have attempted to understand how magnetic ordering and related properties in these oxides depend sensitively on disorder at the cation site. The origin and tendency of cations to disorder and the associated properties are traced to the local structure and ionic sizes.

© 2011 Elsevier Inc. All rights reserved.

## 1. Introduction

$\text{Al}_2\text{O}_3$ ,  $\text{Ga}_2\text{O}_3$  and  $\text{Fe}_2\text{O}_3$  are known to crystallize in the rhombohedral structure. Metastable orthorhombic phases ( $Pna2_1$ ) of these materials are also known [1]. Surprisingly the stable structures of  $\text{AlFeO}_3$  and  $\text{GaFeO}_3$  belong to the non-centrosymmetric chiral space group with an orthorhombic ( $Pna2_1$ ) structure [2–5].  $\text{AlFeO}_3$  and  $\text{GaFeO}_3$  are reported to be ferrimagnetic [5–7]. These materials are also expected to be multiferroic. In view of their unusual properties, we have investigated the structure and magnetic properties of  $\text{AlFeO}_3$  and  $\text{GaFeO}_3$  in detail by carrying out a neutron diffraction study of the structures, along with magnetic and Mössbauer measurements to establish the nature of magnetic properties. Since ionic sizes and disorder appear to play crucial roles in determining the properties of these materials, we have investigated the structure and properties of  $\text{Al}_{0.5}\text{Ga}_{0.5}\text{FeO}_3$  as well. First-principles density functional theory calculations have been carried out to understand the properties of these materials in relation to their structures.

## 2. Experimental

$\text{AlFeO}_3$  and  $\text{GaFeO}_3$  were prepared by the co-precipitation method [7] starting from stoichiometric amounts of  $\text{Fe}_2\text{O}_3$  and Al ( $\text{Ga}_2\text{O}_3$ ) powder. The powders were dissolved separately in conc. HCl to form the chlorides of the metal ion. Respective metal chloride solutions were mixed and stirred for half an hour. After that  $\text{NH}_4\text{OH}$  solution was added drop by drop with continuous stirring until rich precipitation. The precipitate was filtered, washed with distilled water to remove the residual ammonium chloride salt until neutral pH and dried at 80 °C in an air oven for 24 h. The dried powders were grounded, pelletized and sintered at 1350 °C for 2 h in air with a heating rate of 3 °C/min. These oxides were also prepared by the ceramic method by heating mixtures of the component oxides at 1400 °C with a repeated grinding, pelletizing and heating.  $\text{Al}_{0.5}\text{Ga}_{0.5}\text{FeO}_3$  was prepared by heating the appropriate mixture of  $\text{Al}_2\text{O}_3$ ,  $\text{Ga}_2\text{O}_3$  and  $\text{Fe}_2\text{O}_3$  at 1400 °C for 5 h. Other compositions of  $\text{Al}_{1-x}\text{Ga}_x\text{FeO}_3$  were also prepared by the ceramic method. Phase purities of these oxides were confirmed by recording the X-ray diffraction patterns with a Bruker D8 Advance X-ray diffractometer. A software package Fullprof was used to analyze the structural data. Neutron powder diffraction measurements on polycrystalline  $\text{Al}_{1-x}\text{Ga}_x\text{FeO}_3$  samples were carried out over the temperature range of 5–300 K using the five linear position sensitive detector (PSD) based powder diffractometer ( $\lambda=1.2443$  Å). The powdered sample was

\* Corresponding authors. Fax: +91 80 22082766.

E-mail addresses: [sundaresan@jncasr.ac.in](mailto:sundaresan@jncasr.ac.in) (A. Sundaresan), [cnrao@jncasr.ac.in](mailto:cnrao@jncasr.ac.in) (C.N.R. Rao).

placed in a cylindrical vanadium container and a commercial closed cycle helium refrigerator was used for low temperature measurements.

DC magnetization measurements were carried out using a vibrating sample magnetometer in Physical Property Measurement System (PPMS) under zero-field-cooled (ZFC) and field-cooled (FC) condition in the temperature range of 10–330 K under a magnetic field of 100 Oe. Magnetic hysteresis curves were recorded at 5 K in magnetic fields reaching up to 60 kOe. Mössbauer spectra were recorded in transmission mode using  $^{57}\text{Co}$   $\gamma$ -ray source in a Rhodium matrix and multi-channel analyzer. The sample thickness was adjusted so that the Fe content was approximately 10 mg/cm<sup>2</sup>. Calibrations of velocity and isomer shift were performed using  $\alpha$ -iron (Fe) foil. Measurements at low temperatures were carried out using a helium close cycle cooler system attached to the sample chamber.

### 3. Results and discussion

X-ray diffraction measurements on  $\text{AlFeO}_3$  and  $\text{GaFeO}_3$  carried out by us gave the following lattice parameters:  $a=4.9806(3)$  Å,  $b=8.5511(6)$  Å and  $c=9.2403(6)$  Å for  $\text{AlFeO}_3$ ;  $a=5.0814(2)$  Å,  $b=8.7436(3)$  Å and  $c=9.3910(2)$  Å for  $\text{GaFeO}_3$ . The space group of both these oxides is  $Pna2_1$ . X-ray diffraction measurements showed that  $\text{Al}_{0.5}\text{Ga}_{0.5}\text{FeO}_3$  also crystallizes in the  $Pna2_1$  space group with the lattice parameters,  $a=5.0306(1)$  Å,  $b=8.6461(2)$  Å, and  $c=9.3175(2)$  Å. These parameters are in between those of  $\text{AlFeO}_3$  and  $\text{GaFeO}_3$ . A detailed neutron diffraction study was carried on all the three oxides. In Fig. 1, we show Rietveld refined neutron diffraction patterns of  $\text{AlFeO}_3$ ,  $\text{GaFeO}_3$  and  $\text{Al}_{0.5}\text{Ga}_{0.5}\text{FeO}_3$  at 300 K. We give the atomic coordinates of  $\text{Al}_{0.5}\text{Ga}_{0.5}\text{FeO}_3$  in Table 1 since this oxide composition has not

been reported earlier. Based on the diffraction data, we arrive at the crystal and magnetic structures shown in Fig. 2. The crystal structure of these compounds is made up of alternative layers of cations and oxygen ions along the crystallographic  $c$  direction. There are four different sites of Fe and Al/Ga, with Fe1, Fe2, and A2 sites being present in an octahedral environment. The A1 sites are in a tetrahedral environment (Fig. 2). The octahedra are connected to each other by the sharing of edges, whereas the tetrahedron shares oxygen ions at the corners. No edge sharing occurs between the octahedra and tetrahedra. There are eight formula units (40 atoms) per unit cell, in agreement with the earlier reports. The crystal structure remains same down to 5 K. In the  $\text{Al}_{1-x}\text{Ga}_x\text{FeO}_3$  compositions, the unit cell parameters and volume increase linearly with the Ga content as shown in Fig. 3. The unit cell parameters of  $\text{Al}_{1-x}\text{Ga}_x\text{FeO}_3$  show a significant temperature dependence with a change in slope around 150 K, the increase in the parameters becoming even more marked in the 200–250 K range (Fig. 4). It is noteworthy that the  $T_N$  values of  $\text{Al}_{1-x}\text{Ga}_x\text{FeO}_3$  are in the 200–250 K range as will be seen later. The expansion of the lattice at low temperatures is somewhat uncommon, signifying negative thermal expansion.

We have examined the temperature variation of the distortion parameter of the  $\text{Fe1O}_6$ ,  $\text{Fe2O}_6$ , and  $(\text{Al/Ga})_2\text{O}_6$  octahedra and the  $(\text{Al/Ga})_1\text{O}_4$  tetrahedron. The distortion parameter,  $\Delta$ , of a coordination polyhedron  $\text{AO}_N$  (A: Fe1, Fe2, (Al/Ga)1, and (Al/Ga)2 with an average value of the A–O bond length,  $\langle d \rangle$ , is defined as

$$\Delta = (1/N) \sum_1^N \{(d_N - \langle d \rangle) / \langle d \rangle\}^2$$

The temperature dependence of  $\Delta$  was found to be negligible for the (Al/Ga)1 tetrahedron and for all three octahedral sites as shown in Fig. 5 in the case of  $\text{Al}_{0.5}\text{Ga}_{0.5}\text{FeO}_3$ . The octahedral environment of the Fe1 and Fe2 sites is highly distorted while the octahedral (Al/Ga) $_2\text{O}_6$  site is relatively less distorted. The  $\text{AlO}_4$  tetrahedron is not distorted in all the three oxides. The observed distortion in the polyhedra is due to the large difference between ionic radii of  $\text{Fe}^{3+}$  and  $\text{Al}^{3+}$  along with the site disorder caused by mixed occupation of Fe and Al. In the case of  $\text{AlFeO}_3$ , we noticed a slight maximum in  $\Delta$  around 150 K for the octahedral site ( $\text{A2O}_6$ ), but no such maximum was, however, observed in  $\text{Al}_{0.5}\text{Ga}_{0.5}\text{FeO}_3$  and  $\text{GaFeO}_3$ .

The magnetic unit cell dimension of  $\text{Al}_{1-x}\text{Ga}_x\text{FeO}_3$  is the same as the chemical (nuclear) one (Fig. 2). The magnetic structure is collinear ferrimagnetic with the ordered magnetic moment aligned along the crystallographic  $a$  direction. The site occupancies were found not to vary with lowering of temperature. Therefore, the values of the site occupancies as derived from the analysis of the diffraction pattern at 300 K (paramagnetic state) were used for the magnetic structure refinement. At lower temperatures, an increase in the intensity of the fundamental (nuclear) Bragg peaks at lower scattering angles confirms the ferrimagnetic ordering. The moments at Fe1 and Fe3 sites are parallel to each other and aligned antiparallel to the parallel aligned moments at Fe2 and Fe4 sites.

The Néel temperatures of  $\text{AlFeO}_3$ ,  $\text{GaFeO}_3$  and  $\text{Al}_{0.5}\text{Ga}_{0.5}\text{FeO}_3$  are 250, 210 and 220 K, respectively (Fig. 6), with the  $T_N$  decreasing with increasing Ga content. Thus, both magnetic ordering and unit cell parameters vary systematically with the cation size or Ga content. All the three compounds show divergence between the zero-field cooled and field-cooled magnetization data. Ferrimagnetic magnetization of  $\text{Al}_{1-x}\text{Ga}_x\text{FeO}_3$  mainly originates from the difference in Fe occupation at the four inequivalent cation sites. Magnetic ordering occurs due to the cation–oxygen–cation superexchange antiferromagnetic interactions where the strength of the interaction strongly depends on

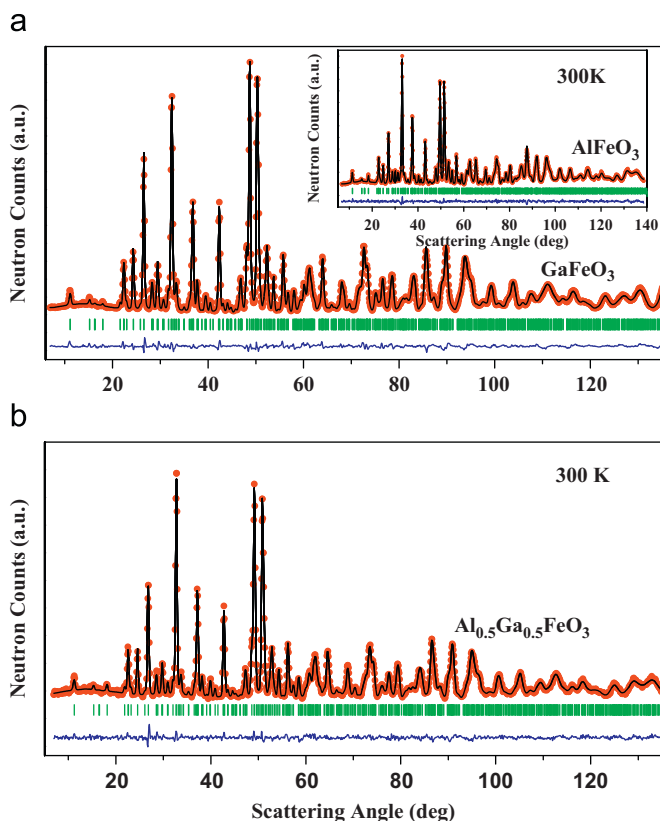


Fig. 1. Rietveld refined neutron diffraction pattern at 300 K for (a)  $\text{GaFeO}_3$  (inset  $\text{AlFeO}_3$ ) and (b)  $\text{Al}_{0.5}\text{Ga}_{0.5}\text{FeO}_3$ .

**Table 1**Atomic coordinates of  $\text{Al}_{0.5}\text{Ga}_{0.5}\text{FeO}_3$  at 300 K (space group:  $Pna2_1$  (orthorhombic),  $a=5.0306(1)$  Å,  $b=8.6461(2)$  Å, and  $c=9.3175(2)$  Å).

Atoms	$x/a$	$y/b$	$z/c$	$B_{\text{iso}}$	Occ.
Fe1/Al/Ga	0.1894(8)	0.1547(7)	0.5829(7)	0.23(2)	0.73(2)/0.16(2)/0.11(2)
Fe2/Al/Ga	0.6721(2)	0.0327(5)	0.7987(9)	0.41(5)	0.71(1)/0.14(1)/0.15(1)
Al1/Ga/Fe	0.1775(5)	0.1513(9)	0	0.52(7)	0.43(2)/0.37(1)/0.20(1)
Al2/Ga/Fe	0.8119(7)	0.1620(9)	0.3050(1)	0.47(3)	0.35(2)/0.34(2)/0.31(2)
O1	0.9768(2)	0.3270(4)	0.4190(9)	0.61(5)	1.0
O2	0.5200(9)	0.4874(9)	0.4356(4)	0.87(6)	1.0
O3	0.6479(2)	0.0002(1)	0.2009(1)	0.59(9)	1.0
O4	0.1556(4)	0.1595(1)	0.1960(8)	0.58(3)	1.0
O5	0.8390(2)	0.1675(2)	0.6703(1)	0.61(9)	1.0
O6	0.5011(2)	0.1696(1)	0.9379(1)	0.44(7)	1.0
$\chi^2$	3.32%				
$R_p$	7.80%				
$R_{\text{wp}}$	8.54%				
$R_{\text{exp}}$	4.40%				
$R_{\text{Bragg}}$	3.34%				

the bond angles and bond lengths. Exchange interaction is strongest for the  $180^\circ$  cation–oxygen–cation bond angle and weakens with the deviation from  $180^\circ$ . The most important pathways for the superexchange antiferromagnetic interactions are Fe1–[O1/O3/O5]–Fe2 and Fe1–[O1/O3]–(Al/Ga)2. The Al1 site involved is less populated by the Fe ions. The strength of superexchange interaction is inversely proportional to the bond length between the magnetic ions. So a decrease in the Néel temperature with Ga content can arise from the increase in the bond lengths associated with it. All the three oxides show magnetic hysteresis at low temperature (5 K) as shown in the insets of Fig. 6.

Mössbauer spectra of the three oxides at 300 K appear as doublets. An analysis of this doublet reveals the paramagnetic nature of the randomly oriented  $\text{Fe}^{3+}$  ions with no exchange interactions. The isomer shift values obtained for this doublet also confirms the presence of iron in ferric state. To ascertain the distribution of Fe at different cation sites, Mossbauer spectra were recorded on the samples at low temperatures using a helium close cycle cooler system attached to the sample chamber. In Fig. 7, we show the Mössbauer spectra of  $\text{AlFeO}_3$ ,  $\text{Al}_{0.5}\text{Ga}_{0.5}\text{FeO}_3$  and  $\text{GaFeO}_3$  at 10 K. The spectra were analyzed using the WinNormos-for-Igor Mössbauer spectra fitting software sold by WissEl GmbH, Starnberg, Germany. The hyperfine parameters were obtained by fitting theoretical subspectral curves to experimental data with Lorentzian line shapes to deconvolute Fe sites in the spectra. The areas of the lines in the hyperfine spectra were constrained to be in the ratio 3:2:1:1:2:3. In Table 2 we give the refined parameters. The isomer shifts obtained at 10 K are found to be 0.2–0.35 mm/s relative to  $\alpha$ -iron for the three samples, consistent with the ferric state in oxide materials [8–10].

The site occupancies of the three octahedral sites Fe1, Fe2, (Al/Ga)2 and one tetrahedral site (Al/Ga)1 were determined from the respective areas of different Fe sites by the method described in the literature [11]. From this analysis, the Fe site occupancies of the Fe1, Fe2, A2 and A1 sites in  $\text{AlFeO}_3$  are found to be 50, 26, 17 and 7, respectively. The Fe site occupancy values for  $\text{Al}_{0.5}\text{Ga}_{0.5}\text{FeO}_3$  and  $\text{GaFeO}_3$  are, respectively, 38, 34, 19, 9 and 50, 23, 17, 10. The magnetic hyperfine field values in these oxides correspond to the ferric state and the hyperfine fields at the Fe1, Fe2, (Al/Ga)2, and (Al/Ga)1 sites decreases with the Ga content in  $\text{Al}_{1-x}\text{Ga}_x\text{FeO}_3$  as shown in Fig. 8.

In order to understand the magnetic properties of these oxides in relation to their structure, we have carried out first-principles calculations based on density functional theory (DFT) with a spin-density dependent exchange correlation energy functional of a

generalized gradient approximated (GGA) (PerdewWang 91 (PW 91)) form [12] as implemented in the Vienna ab initio Simulation Package (VASP) [13,14]. The projector augmented wave (PAW) method [15] was used to capture interaction between ionic cores and valence electrons. An energy cutoff of 400 eV was used for the plane wave basis and integrations over the Brillouin were carried out using a regular  $4 \times 4 \times 4$  mesh of  $k$ -points. Structure was optimized to minimum energy using Hellman–Feynman forces, while maintaining the lattice constants at their experimental values. Minimum energy states with different magnetic ordering were obtained through appropriate initialization of the spins on Fe sites.

Before we undertake first-principles calculations, we shall briefly revisit the crystal structure of  $\text{AlFeO}_3$  (Fig. 9). There are four different Wyckoff sites of cations labeled Fe1, Fe2 (predominantly occupied by iron), Al1 and Al2 (predominantly occupied by aluminum). The occupancy factors of the cation sites are given in Table 3. Cation site disorder here means occupation of Fe site by an Al cation or vice versa, arising from an interchange of Al and Fe atoms in the perfectly ordered structure. From the observed data of occupancies of cation sites at low temperatures, disorder arises with highest probability through interchange in the positions of Fe and Al cations at Fe2 and Al2 sites. We have simulated the disordered structure (D) obtained by interchanging one Al at Al2 site with one Fe atom at Fe2 site (in one unit cell, amounting to 12.5% anti-site defects), along with the perfectly ordered structure (O). Symmetry of the structure permits a non-zero polarization along the  $c$ -axis, consistent with the known piezoelectric properties.

Disorder, magnetic ordering and stability of  $\text{AlFeO}_3$  were studied theoretically. From the energies of the ferromagnetically and antiferromagnetically ordered states of  $\text{AlFeO}_3$  (Table 4), it becomes clear that the antiferromagnetic state (AFM) is more stable than the ferromagnetic (FM) one in the chemically ordered case. Noting that there are eight Fe ions with six-fold coordination in the unit cell, an estimate of the exchange coupling in a model with nearest neighbor interaction of constant spins is about 0.076 eV, significantly higher than the experimental magnetic transition temperature. This can be rationalized through closer examination of the magnetically ordered states. Magnetic moments of the various Fe ions change significantly (Tables 5 and 6) with change in their ordering, resulting in  $\text{Fe}^{3+}$  in the low-spin state in the FM-ordered state. Thus, interpretation of the estimate of exchange interaction is little tricky when compared with experimental magnetic transition. As the low-spin state of  $\text{Fe}^{3+}$  is known to be rare in nature, FM state of  $\text{AlFeO}_3$  is indeed much higher in energy than the AFM one.

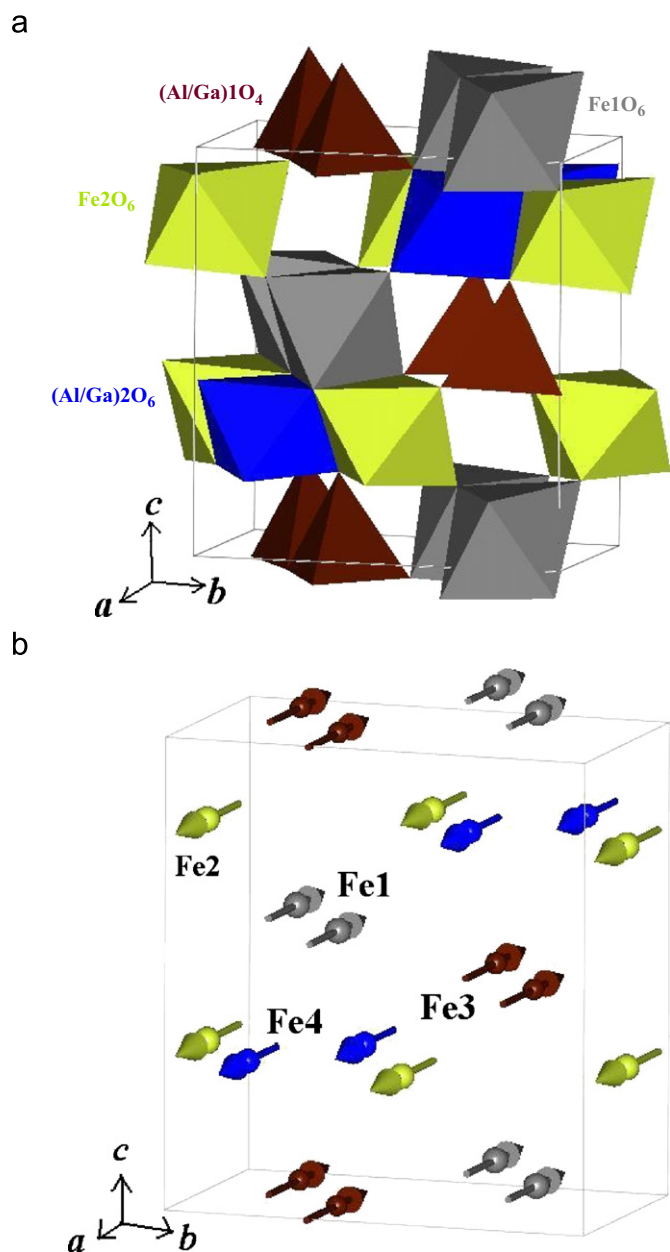


Fig. 2. (a) Crystal structure and (b) magnetic structure of  $\text{Al}_{1-x}\text{Ga}_x\text{FeO}_3$  ( $x=0, 0.5, 1$ ).

A rather interesting change is seen in our analysis when we introduce the anti-site disorder between Fe2 and Al2. First of all, the difference in energies of FM and AFM states (Table 4) becomes much smaller, with an estimated strength of the nearest neighbor exchange interaction of about 0.031 eV, much smaller than that in the chemically ordered configuration. Secondly, the magnetic moments (Tables 5 and 6) change significantly only of the Fe ion located at the Al2 site, indicating its low-spin state in the FM ordering. Our result for the exchange interaction in this case in comparison with experimental  $T_N$  is an overestimate, typical of DFT calculations. We also note that the magnetic moment on each  $\text{Fe}^{3+}$  ion varies with the site in both the AFM and FM states, and in this sense the system is ferrimagnetic with a rather small effective magnetic moment, as seen experimentally. The energy of magnetic ordering with lowest energy in the disordered case is 0.58 eV higher than that in the ordered case, giving an estimate of energy of an anti-site defect. Interestingly, FM ordering in the

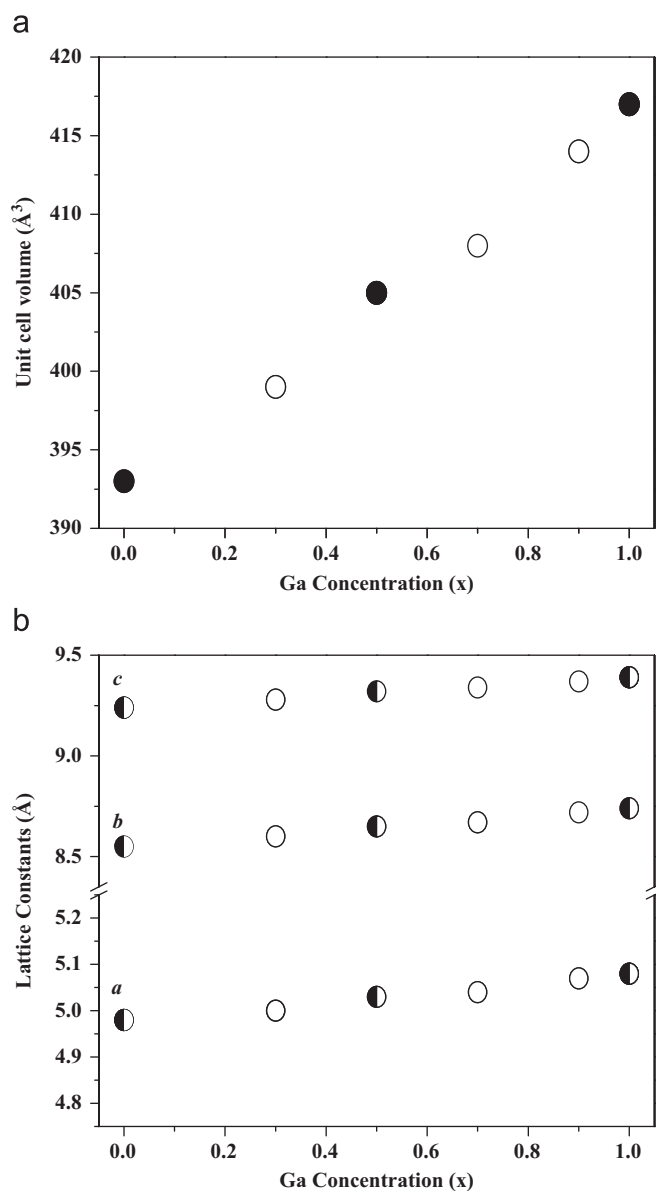


Fig. 3. Variation of lattice constants and unit cell volume in  $\text{Al}_{1-x}\text{Ga}_x\text{FeO}_3$  with Ga content at 300 K obtained from neutron diffraction measurements (data shown as closed circles). Data from X-ray diffraction are shown as open circles.

disordered state is lower in energy than the FM ordering in the chemically ordered state.

We shall now examine these results in terms of the electronic and atomic structure and how they are affected by anti-site disorder.  $\text{Fe}^{3+}$  ion has an  $[\text{Ar}] 3d^5$  electronic configuration and an octahedral crystal field results in a splitting of the degeneracy of its  $d$  state into  $t_{2g}$  and  $e_g$  states. Intra-atomic exchange interaction breaks the spin degeneracy and all  $5d$  electrons occupy states with the same spin. For  $d^5$  configuration, superexchange interaction via O is strongly antiferromagnetic, particularly when  $\text{Fe}-\text{O}-\text{Fe}$  bond angles are close to  $180^\circ$ , and hence the ground state exhibits an AFM ordering. Ideally, such electronic structure would give a magnetic moment of  $5 \mu_B$  per Fe ion, corresponding to the high-spin state. Our simulations, however, give a moment of about  $4 \mu_B$  per Fe ion due to a strong hybridization between the  $d$  states of Fe and the  $p$  states of O (see Figs. 10 and 11), similar to that in  $\text{BiFeO}_3$  [16]. Since we have not included any on-site correlation (Hubbard  $U=0$ ), our  $d$  band

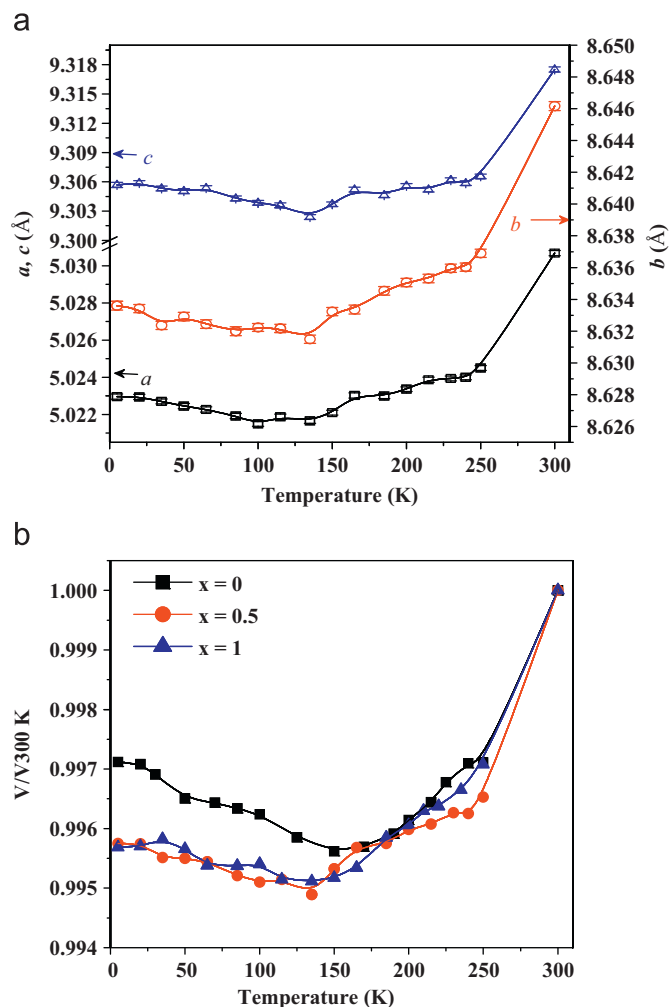


Fig. 4. (a) Variation of lattice parameters of  $\text{Al}_{0.5}\text{Ga}_{0.5}\text{FeO}_3$  with temperature and (b) variation of cell volume of  $\text{Al}_{1-x}\text{Ga}_x\text{FeO}_3$  ( $x=0, 0.5, 1$ ) with temperature.

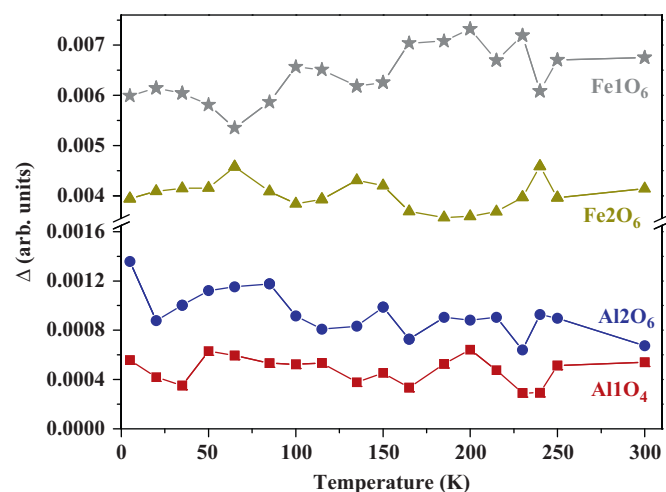


Fig. 5. Temperature dependence of distortion parameter of polyhedral in  $\text{Al}_{0.5}\text{Ga}_{0.5}\text{FeO}_3$ .

widths are expected to be overestimated. If the crystal field splitting is larger than the exchange coupling,  $\text{Fe}^{3+}$  can be in the low-spin state, as seen from our simulations of (a) FM state in

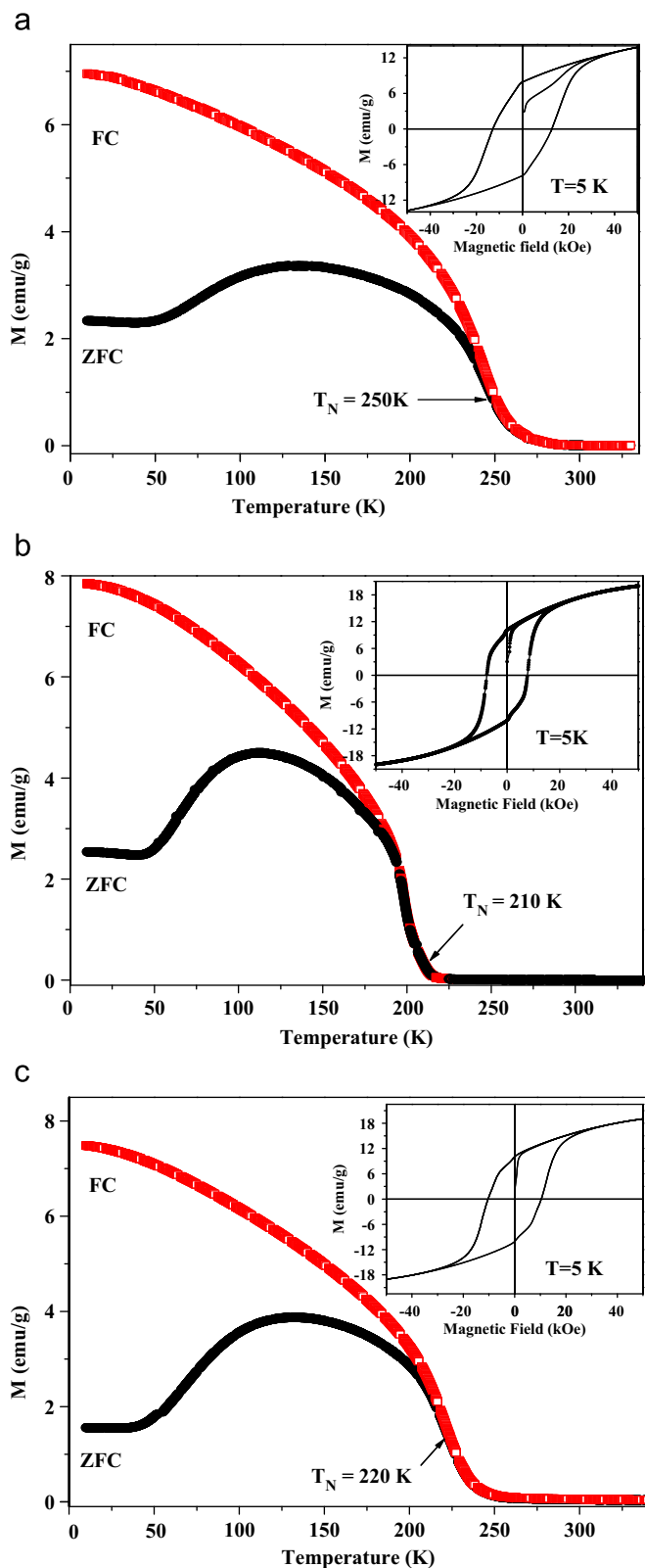
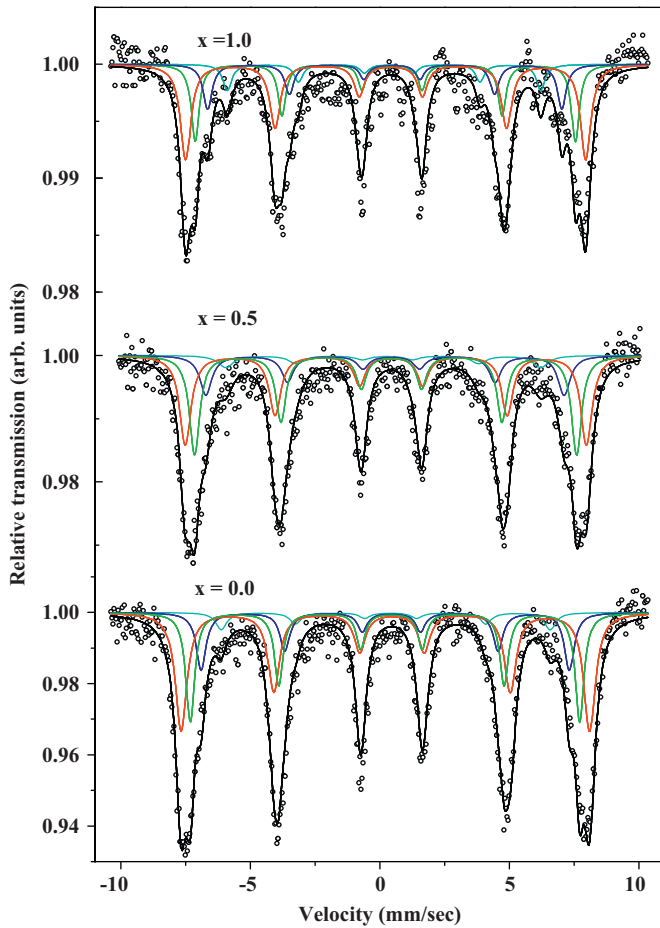


Fig. 6. Temperature dependent magnetization of (a)  $\text{AlFeO}_3$ , (b)  $\text{GaFeO}_3$  and (c)  $\text{Al}_{0.5}\text{Ga}_{0.5}\text{FeO}_3$  under field cooled (FC) and zero-field-cooled (ZFC) conditions. Magnetic hysteresis at 5 K is shown in the inset.

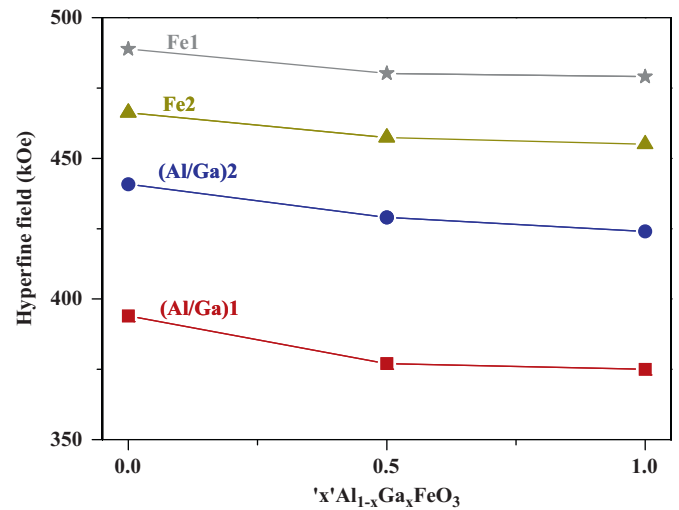
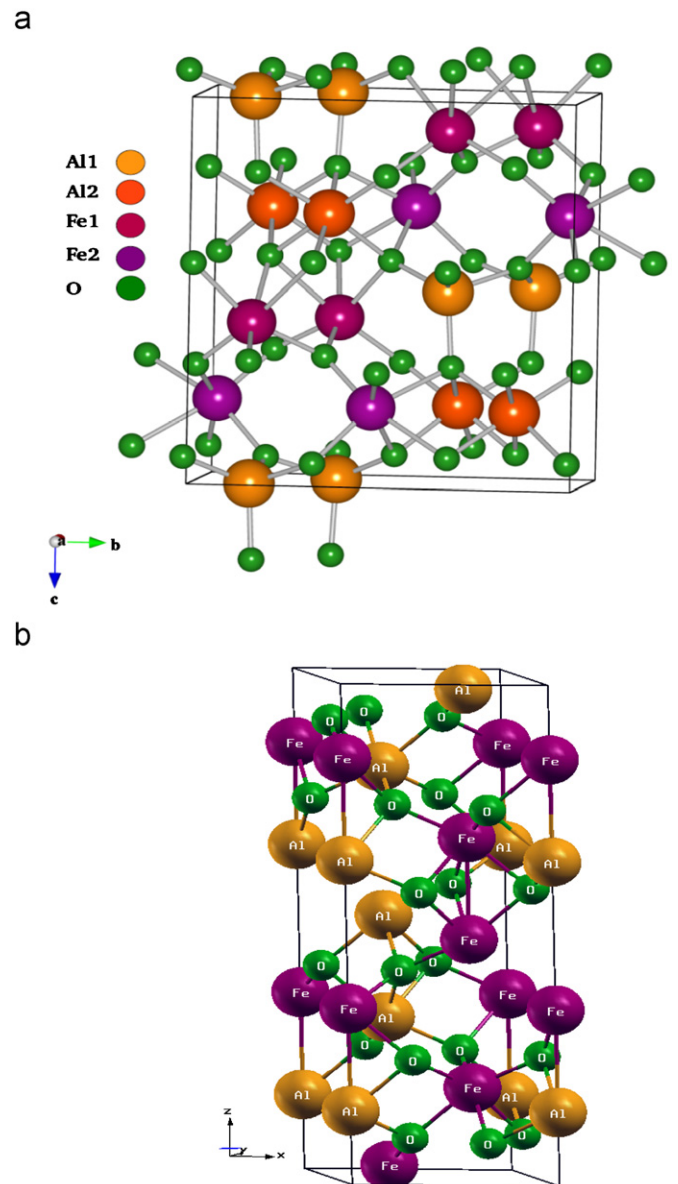
the chemically ordered case, and (b) Fe populating Al2 site of the FM state in the disordered case. In the AFM or FM states, however,  $\text{Fe}^{3+}$  is always in the high-spin state irrespective to its site, consistent with its greater stability. This is also reflected in a small gap

Fig. 7. Mössbauer spectra on  $\text{Al}_{1-x}\text{Ga}_x\text{FeO}_3$  at 10 K.

**Table 2**  
Mössbauer parameters for  $\text{Al}_{1-x}\text{Ga}_x\text{FeO}_3$  system at 10 K.

Compound formula	Site	$\delta$ (mm/s)	$\Delta E_Q$ (mm/s)	$B_{\text{hf}}$ (kOe)	Fe occupancy (%)
$\text{AlFeO}_3$	Fe1	0.340(3)	-0.257(5)	489(1)	50
	Fe2	0.321(4)	-0.252(7)	466(1)	26
	Al2	0.326(7)	-0.24(1)	441(1)	17
	Al1	0.32(2)	-0.19(4)	394(1)	7
$\text{Al}_{0.5}\text{Ga}_{0.5}\text{FeO}_3$	Fe1	0.333(5)	-0.203(8)	480(1)	38
	Fe2	0.332(4)	-0.227(8)	457(1)	34
	(Al/Ga)2	0.32(1)	-0.24(2)	429(1)	19
	(Al/Ga)1	0.21(1)	-0.16(2)	377(1)	9
$\text{GaFeO}_3$	Fe1	0.32(1)	-0.20(3)	479(1)	50
	Fe2	0.339(7)	-0.26(3)	455(1)	23
	Ga2	0.33(2)	-0.28(5)	424(2)	17
	Ga1	0.25(2)	-0.20(7)	375(1)	10

in the electronic structure (Fig. 11), which is typically underestimated in DFT calculations. We point out that the simulated gap may become more pronounced when on-site correlation (through Hubbard  $U$  correction) is included. A non-zero density of states at the Fermi energy in the AFM state in the disordered case arises from the states localized on  $\text{Fe}^{3+}$  at Al2 site and is not expected to make it metallic. Finally, a larger exchange energy  $E_{\text{xc}}$  in the disordered FM state than that in the ordered FM state is responsible for its high-spin state and its greater stability.

Fig. 8. Variation of Hyperfine field ( $B_{\text{hf}}$ ) with 'x' in  $\text{Al}_{1-x}\text{Ga}_x\text{FeO}_3$ .Fig. 9. Structure of  $\text{AlFeO}_3$  in (a) orthorhombic and (b) corundum structures.

**Table 3**  
Occupancy factors of AlFeO<sub>3</sub> at room temperature from neutron diffraction studies (from the recent study).

Cation site	Occupancy by Fe	Occupancy by Al
Fe1	0.83(2)	0.17(2)
Fe2	0.81(1)	0.19(1)
Al1	0.14(1)	0.85(1)
Al2	0.26(2)	0.74(2)

**Table 4**  
Energetics of magnetic configuration in AlFeO<sub>3</sub>.

Order/disorder	Total energy of magnetic configuration (eV)		
	AlFeO <sub>3</sub> —FM	AlFeO <sub>3</sub> —AFM	GaFeO <sub>3</sub> —AFM
Ordered	−297.02	−300.67	−270.75
Disordered	−298.59	−300.09	−270.64

**Table 5**  
Total magnetic moments in AlFeO<sub>3</sub>.

Order/disorder	Total magnetic moment ( $\mu_B$ )	
	FM	AFM
Ordered	7.80	0.058
Disordered	22.87	−0.002

**Table 6**  
Magnetic moments of individual Fe ions ( $\mu_B$ ) in AlFeO<sub>3</sub>.

Atom no.	Cation site	Magnetic moment ( $\mu_B$ )			
		FM		AFM	
		Order	Disorder	Order	Disorder
1	Fe1	1.26	3.85	3.59	3.69
2	Fe1	1.26	−3.20	3.59	3.40
3	Fe1	1.26	3.12	3.59	3.71
4	Fe1	1.26	3.77	3.59	3.58
5	Fe2/Al2	0.50	1.27	−3.57	−3.72
6	Fe2	0.50	3.70	−3.57	−3.59
7	Fe2	0.50	3.66	−3.57	−3.58
8	Fe2	0.50	3.81	−3.57	−3.54

We now examine the relation between structure and magnetic ordering as well as anti-site disorder. From the bond lengths of oxygen to Fe and Al ions at the Fe2 and Al2 sites (Table 7), a characteristic feature becomes evident. The Fe2 site prefers dichotomous (bi-modal distribution) of bond lengths while the Al2 site exhibits uniformity in bond lengths. In the relaxed structures (see Tables 5 and 7), we observe that the bond lengths change considerably with the change in magnetic ordering implying a strong spin–phonon coupling in the system (note that we report bond lengths for Fe and Al are at Fe2 and Al2 sites, respectively, in the ordered state; Fe and Al are at Al2 and Fe2 sites respectively in the disordered state). Our results clearly bear that (a) a high-spin state of Fe<sup>3+</sup> is energetically favorable (lower) than the low-spin state, and (b) Fe–O bonds are longer when Fe<sup>3+</sup> is in the high-spin state, a feature intimately linked with disorder,

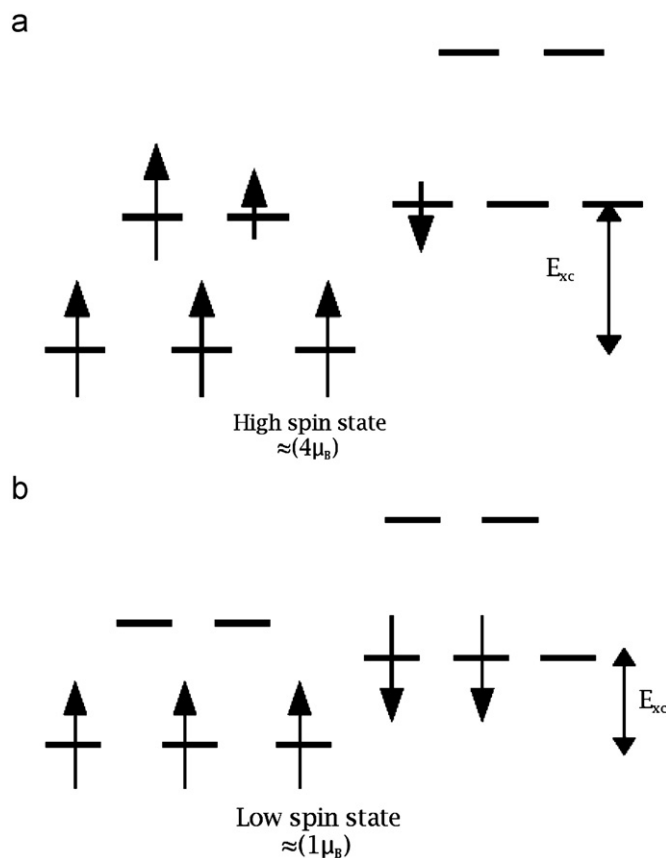


**Fig. 10.** (a) High-spin and (b) low-spin states.

since the Shannon–Prewitt radius of Fe<sup>3+</sup> in the low-spin state is close to that of Al<sup>3+</sup> in octahedral coordination, the FM state in the disordered case is significantly lower in energy because only Fe<sup>3+</sup> at the Al2 site takes the low-spin state and Fe<sup>3+</sup> at other sites are in the high-spin state. This results in longer Fe–O bond-lengths in the high-spin configuration, reflected in the Fe–O bonds in the AFM state with Fe<sup>3+</sup> taking the high-spin state.

We have determined the energetics of AlFeO<sub>3</sub> in perovskite and corundum structures (see Fig. 9). While Fe is found to prefer A site with a high-spin state and G-AFM ordering, the energy of the cubic perovskite structure is almost 3 eV higher than the observed one. Secondly, Fe<sup>3+</sup> randomly occupying Al sites in the corundum structure takes the low-spin state (due to size mismatch), and hence AlFeO<sub>3</sub> in the corundum structure is higher in energy by about 84 meV/formula unit. Thus, we understand the stability of the observed structure is partly due to the distinct sites associated with Al and Fe.

We have examined disorder, magnetic ordering and stability of GaFeO<sub>3</sub>. The importance of site disorder and local distortion in determining the magnetic properties of this oxide has been recognized [17]. Because of the mismatch in the ionic radii of Fe<sup>3+</sup> in high-spin state and Al<sup>3+</sup>, anti-site disorder in AlFeO<sub>3</sub> is relatively weak. In contrast, the radius of Fe<sup>3+</sup> in high-spin state ( $R=0.62$  Å) is close to that of Ga<sup>3+</sup> in octahedral coordination, hinting a greater degree of anti-site disorder in GaFeO<sub>3</sub>. From our calculations on GaFeO<sub>3</sub> we find that (a) its AFM state is lower in energy than the FM one in both the ordered and disordered cases with a slightly larger magnetic moment in the latter. (b) Within a DFT-description, FM ordering does not occur in a self-consistent solution. (c) In the AFM state, magnetic moments at Fe1 and Fe2 sites are not of the same magnitude giving a weak magnetic

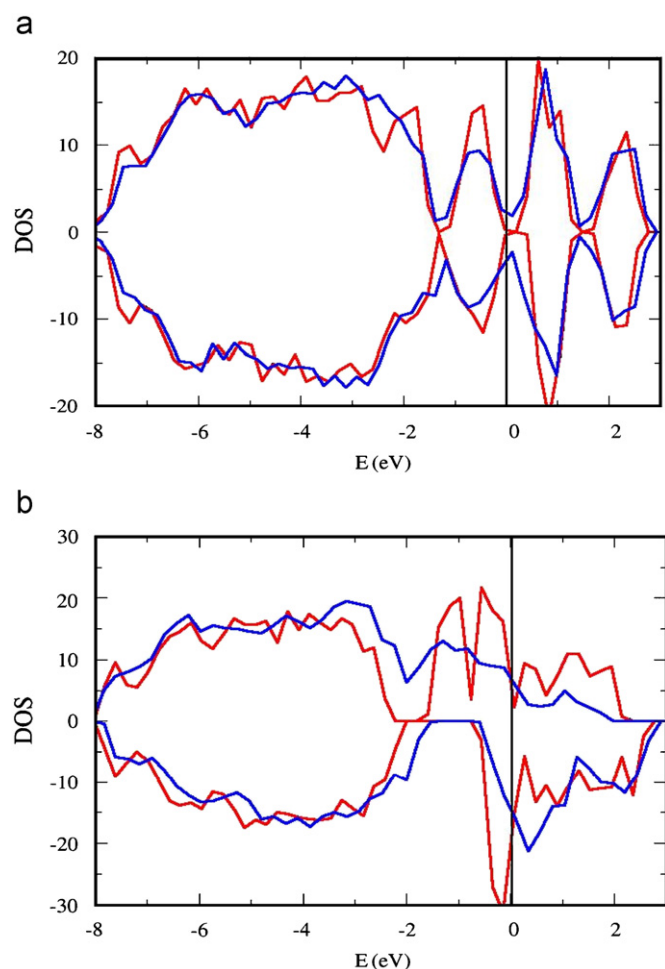


**Fig. 11.** Ordered state shown in red and disordered state shown in blue. Comparison of electronic density of states for ordered and disordered states for system in (a) AFM and (b) FM configurations. (For interpretation of the references to color in this figure legend, the reader is referred to the web version of this article.)

**Table 7**

Fe–O and Al–O bond lengths (Å) in AlFeO<sub>3</sub>.

State	Chemically ordered		Chemically disordered	
	<i>L</i> (Fe–O)	<i>L</i> (Al–O)	<i>L</i> (Fe–O)	<i>L</i> (Al–O)
FM	1.87	1.90	1.85	1.86
	1.87	1.92	1.93	1.87
	1.97	1.93	1.95	1.91
	2.04	1.96	1.97	1.95
	2.06	1.96	1.97	2.02
	2.11	2.02	1.99	2.05
AFM	1.83	1.88	1.90	1.85
	1.89	1.90	2.02	1.86
	1.99	1.92	2.02	1.90
	2.10	1.94	2.03	1.95
	2.18	1.95	2.05	2.05
	2.24	1.97	2.09	2.07

moment effectively. (d) The energy difference between the AFM states in the disordered and ordered cases is only 36 meV/formula unit (as opposed to 73 meV/formula unit of AlFeO<sub>3</sub>). Thus, we

expect anti-site disorder in GaFeO<sub>3</sub> to be more prominent than in AlFeO<sub>3</sub>. Electronic structure of GaFeO<sub>3</sub> is qualitatively similar to that of AlFeO<sub>3</sub>.

#### 4. Conclusions

X-ray and neutron diffraction of the Al<sub>1-x</sub>Ga<sub>x</sub>FeO<sub>3</sub> family of oxides show that they all crystallize with an orthorhombic structure with the space group, *Pna*2<sub>1</sub>. The unit cell parameters and volume increase with the Ga content and show a marked increase around the 200 K region. The distortion parameters of the various octahedra do not show significant temperature dependence. The chemical and magnetic unit cells of these oxides are the same and all three oxides are ferrimagnetic. Mössbauer spectroscopy gives useful information on-site occupancies and the hyperfine field decreases with increasing Ga content.

Our first-principles calculations show (i) greater anti-site disorder in GaFeO<sub>3</sub> than in AlFeO<sub>3</sub> due to better matching of ionic radii of Fe and Ga, (ii) weak magnetic moment arising from the difference in effective magnetic moments of Fe<sup>3+</sup> at Fe1, Fe2 and Al2 sites, and (iii) the presence of strong spin–phonon coupling arising from a large difference in ionic radii of Fe<sup>3+</sup> in high and low-spin states (0.645 and 0.55 Å, respectively). Both disorder and magnetic properties are intimately related to the local structure that can be explained in terms of ionic sizes.

#### References

- [1] K. Kelm, W. Mader, Z. Anorg. Allg. Chem. 631 (2005) 2383.
- [2] F. Bouree, J.L. Baudour, E. Elbadraoui, J. Musso, C. Laurent, A. Rousset, Acta Crystallogr. B52 (1996) 217.
- [3] L.F. Cotica, S.N. De Medeiros, I.A. Santos, A. Paesano Jr., E.J. Kinast, J.B.M. Da Cunha, M. Venet, D. Garcia, J.A. Eiras, Ferroelectrics 338 (2006) 241.
- [4] L.F. Cotica, I.A. Santos, M. Venet, D. Garcia, J.A. Eiras, A.A. Coelho, Solid State Commun. 147 (2008) 123.
- [5] K. Sharma, V.R. Reddy, D. Kothari, A. Gupta, A. Banerjee, V.G. Sathe, J. Phys.: Condens. Matter 22 (2010) 146005.
- [6] R.B. Frankel, N.A. Blum, S. Foner, A.J. Freeman, M. Schieber, Phys. Rev. Lett. 15 (1965) 958.
- [7] M.E. Villafuerte-Castrejón, E. Castillo-Pereyra, J. Tartaj, L. Fuentes, D. Bueno-Baqués, G. González, J.A. Matutes-Aquino, J. Magn. Magn. Mater. 272 (2004) 837.
- [8] K.U. Kang, S.B. Kim, S.Y. An, S.-W. Cheong, C.S. Kim, J. Magn. Magn. Mater. 304 (2006) e769.
- [9] W. Kim, J.H. We, S.J. Kim, C.S. Kim, J. Appl. Phys. 101 (2007) 09M515.
- [10] J.H. We, S.J. Kim, C.S. Kim, IEEE. Trans. Magn. 42 (2006) 2876.
- [11] G. Amthauer, H. Annersten, S.S. Hafner, Z. Kristallogr. 143 (1976) 14.
- [12] J.P. Perdew, J.A. Chevary, S.H. Vosko, K.A. Jackson, M.R. Pederson, D.J. Singh, C. Fiolhais, Phys. Rev. B 46 (1992) 6671.
- [13] G. Kresse, J. Hafner, Phys. Rev. B 47 (1993) R558.
- [14] G. Kresse, J. Furthmiller, Phys. Rev. B 54 (1996) 11169.
- [15] G. Kresse, D. Joubert, Phys. Rev. B 59 (1999) 1758.
- [16] J.E. Neaton, C. Ederer, U.V. Waghmare, N.A. Spaldin, K.M. Rabe, Phys. Rev. B 72 (2005) 14104.
- [17] Myung Joon Han, Taisuke Ozaki, Jaejun Yu, Phys. Rev. B 75 (2007) 060404 R.